Check for updates

^{129}I and ^{236}U distribution in the subpolar North Atlantic unravels water mass provenance in AR7W and A25 lines

Lisa G. T. Leist[1]*, Maxi Castrillejo[2], John Norton Smith[3], Marcus Christl[4], Christof Vockenhuber[4], Antón Velo[5], Pascale Lherminier[6] and Núria Casacuberta[1,4]

[1]Department of Environmental Systems Science, Institute of Biogeochemistry and Pollutant Dynamics, Eidgenössische Technische Hochschule (ETH) Zürich, Zurich, Switzerland, [2]Institute of Earth Sciences, University of Lausanne, Lausanne, Switzerland, [3]Bedford Institute of Oceanography, Fisheries and Oceans Canada, Dartmouth, NS, Canada, [4]Laboratory of Ion Beam Physics, Department of Physics, ETH Zurich, Zurich, Switzerland, [5]Instituto de Investigacións Mariñas, IIM-CSIC, Vigo, Spain, [6]Laboratoire d'Océanographie Physique et Spatiale (LOPS), University of Brest, CNRS, Ifremer, IRD, IUEM, Plouzané, France

The subpolar North Atlantic (SPNA) is crucial in the global ocean circulation system and one of the few regions where deep convection occurs. The intermediate and deep waters formed in the SPNA have long been investigated, yet their sources and pathways are not fully understood. In this study, we employ a combination of two radionuclide tracers, namely, ^{129}I and ^{236}U, to understand water mass provenance and mixing in the SPNA. The concentrations measured between Portugal and Greenland and across the Labrador Sea in 2020/2021 agreed with previously observed tracer distributions. The highest tracer concentrations were measured in the East Greenland Current (EGC), Denmark Strait Overflow Water (DSOW), and, to a lesser extent, in the eastward-flowing Labrador Sea Water (LSW). In contrast, waters of southern origin such as the North East Antarctic Bottom Water and North East Atlantic Central Water (ENACW) carried comparably smaller amounts of ^{129}I. By using a binary mixing model, we estimated that the EGC contains about 29%−32% of the Polar Surface Water outflowing the Fram Strait. DSOW was mainly derived from 20% to 35% Return Atlantic Water and mixed with LSW. The Iceland Scotland Overflow Water (ISOW) evolved into North East Atlantic Deep Water in the Irminger and Labrador seas primarily by mixing with LSW and, to a lesser extent, with DSOW. The ^{129}I and ^{236}U binary mixing approach was less conclusive for LSW, reaching the current limitation of the model. This study suggests potential benefits and limitations of using ^{129}I and ^{236}U to investigate the mixing and provenance of water masses in the SPNA.

1 Introduction

1.1 The subpolar North Atlantic

The subpolar North Atlantic (SPNA) has been recognized as key region for intermediate and deep-water formation since the last century e.g., Clarke and Gascard (1983); Pickart (1992). As such, the SPNA largely contributes to the formation of the southward flowing lower limb of the Atlantic Meridional Overturning Circulation (AMOC) by conversion of shallow northward flowing warm subtropical waters into colder, fresher, and denser waters (Frajka-

Williams et al., 2019; Weijer et al., 2022; Lozier, 2023). The AMOC plays a major role in the climate system due to its great capacity to distribute heat and carbon. Thus, understanding its dynamics is of paramount importance (Zou et al., 2023; Lozier et al., 2019; Rousi et al., 2021). Mooring arrays, floats, and repeated hydrographic expeditions, such as the AR7W line in the Labrador Sea and the OVIDE Line in the central SPNA (Figure 1, red squares), closely monitor the AMOC variability and strength (Li et al., 2021; García-Ibáñez et al., 2018; Lavender et al., 2005; Frajka-Williams et al., 2019) as it may weaken or even collapse within this century (Ditlevsen and Ditlevsen, 2023). The main contributions to the
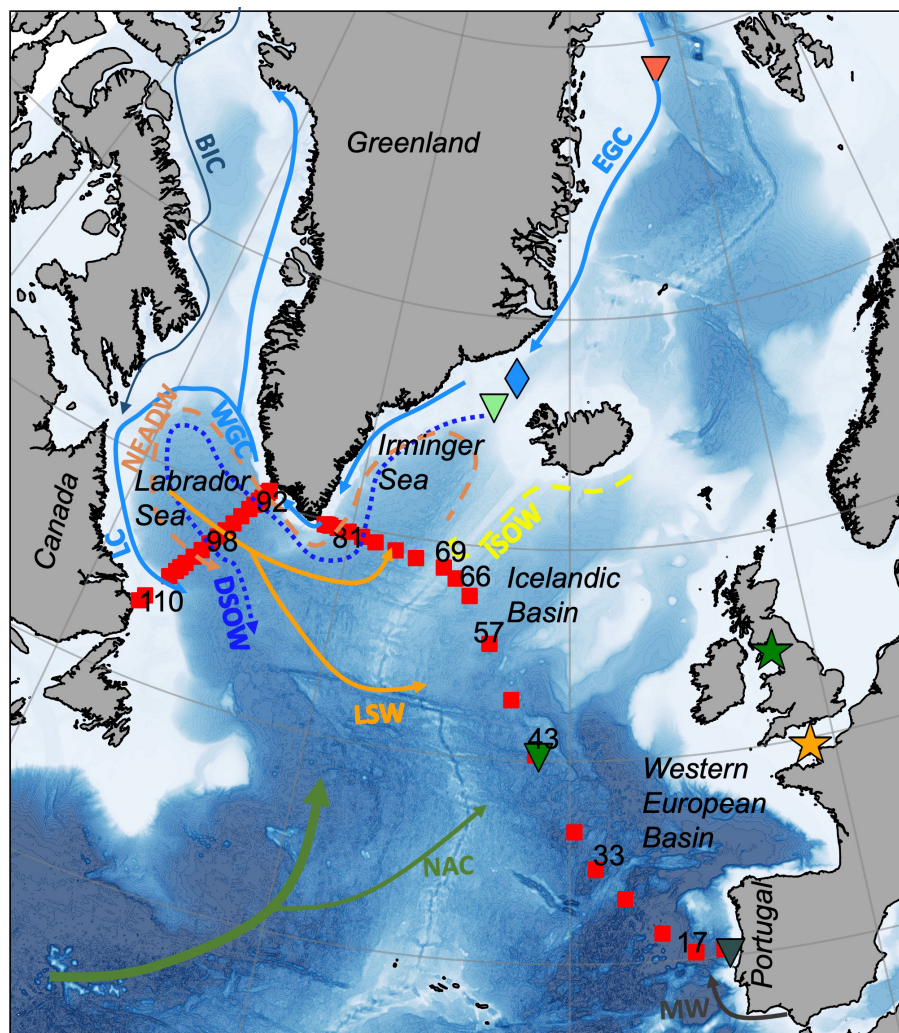
FIGURE 1
Study area, including the oceanographic transects AR7W and A25 sampled in 2020/2021. Red squares represent the location of the sampled stations, and their corresponding station numbers (not all were included to avoid too many labels). Arrows represent the schematic water mass circulation adapted from Daniault et al. (2016). The location of the nuclear fuel reprocessing plants of La Hague and Sellafield is represented by green and orange stars, respectively. The sampling locations of the water mass endmembers are indicated by triangles, and the endmember tracer concentration can be found in Supplementary Table S1. The blue diamond MG17 is a single EGC sample, published by Dale et al. (2024). AAW, Arctic Atlantic Water; BIC, Baffin Island Current; ENACW, Eastern North Atlantic Central Waters; DSOW, Denmark Strait Overflow Water; EGC, East Greenland Current; ISOW, Iceland Scotland Overflow Water; LC, Labrador Current; LSW, Labrador Sea Water; MW, Mediterranean Water; NAC, North Atlantic Current; NCC, Norwegian Coastal Current; NEABW, North East Atlantic Bottom Water; NRP, nuclear reprocessing plant; PSW, Polar Surface Water; WGC, West Greenland Current.

lower limb of AMOC are the Labrador Sea Water (LSW), the Denmark Strait Overflow Water (DSOW), and the Iceland Scotland Overflow Water (ISOW) (Figure 1). In the Labrador Sea, the annual winter convection produces new LSW to a maximum depth of about 2000 m (Yashayaev, 2024). Nordic overflows entering through the Denmark Strait near Greenland (i.e., DSOW) and the Iceland–Scotland sills (i.e., ISOW) fill bottom or deeper depths, respectively (e.g., Bower et al., 2019, 2009).

Ongoing AMOC research is trying to better understand the water mass structure, pathways, mixing, and origin (Zou et al., 2023)—for example, the Deep Western Boundary Current is broadly seen as the main mechanism to transport recently ventilated LSW and Nordic overflows to lower latitudes. However, tracer and float observations indicate intense re-circulation of waters and branching off the boundary current, resulting in extensive eastward intrusion of North Atlantic Deep Water (Susan Lozier et al., 2022). Furthermore, LSW has been shown to recirculate within the subpolar gyre and cross the Reykjanes Ridge into the eastern SPNA (Lavender et al., 2005; Lozier et al., 2013; Susan Lozier et al., 2017). The composition and origin of the above-mentioned waters are still a matter of investigation as it is their mixing with water masses formed south of the subpolar region.

1.2 Anthropogenic radionuclides as tracers of ocean circulation

Since the 1990s, anthropogenic radionuclides such as ^{137}Cs, ^{90}Sr, and ^{3}H have been used to track the Atlantic waters flowing within the Arctic and North Atlantic regions (Dahlgaard et al., 1995; Livingston and Anderson, 1983; Smith et al., 1998). Other than the global fallout input following the atmospheric nuclear bomb tests, the main source of these radionuclides are the liquid releases from the two European nuclear reprocessing plants in Sellafield, UK, and La Hague, F (green and orange stars in Figure 1). The point-like radionuclide source

which starts at the North Sea has been labeling the Atlantic waters entering the Arctic region and flowing back to the SPNA, allowing the pathways of Atlantic-sourced waters to be traced and the transport times and mixing to be estimated (Raisbeck and Yiou, 1999; Kershaw and Baxter, 1995; Alfimov, 2004; Smith et al., 1998; Smith, 2005; Smith et al., 2011). Among these radionuclides, the long-lived ^{129}I emerged as a powerful tracer in the 1990s owing to advances in accelerator mass spectrometry (AMS), allowing ^{129}I determinations in less than 1 L of sample (Christl et al., 2023; Vockenhuber et al., 2015; Christl et al., 2013). The fact that the discharged amounts (^{129}I: >5,000 kg, ^{236}U: >100 kg) (Aldahan et al., 2007; Christl et al., 2015b, a; He et al., 2013) were documented and that they increased considerably after the 1990s (Figure 2A) provided a unique opportunity to resolve transport timescales of tracer-labeled waters beyond the North Sea. Further developments in AMS permitted the measurement of another long-lived radionuclide, ^{236}U, which when combined with ^{129}I resulted in a valuable tool to trace the water exchange within and between the Atlantic and Arctic Oceans (Casacuberta et al., 2016, 2018; Castrillejo et al., 2018). The combination of ^{129}I and ^{236}U serves as a unique dye for water masses thanks to their long half-lives (^{129}I: $T_{1/2}$ = 15.7 Myr, ^{236}U: $T_{1/2}$ = 23.5 Myr), their negligible natural abundance, and their conservative behavior in open ocean waters (Aldahan et al., 2007; Sakaguchi et al., 2012).

The combination of ^{129}I and ^{236}U highlights the strength of using tracers with different input histories, as the tracer signature leaving the North Sea is unique for a given year (Casacuberta and Smith, 2023). Although ^{129}I is mostly released from La Hague (Figure 2A) and ^{236}U comes predominantly from Sellafield (Figure 2B), both releases mix at the North Sea before being transported northward to the Barents Sea Opening and the Fram Strait (Smith et al., 2011; Casacuberta et al., 2018; Wefing et al., 2019; Castrillejo et al., 2018). In the Arctic Ocean, these two tracers have recently proven their suitability to estimate pathways, transit times, and mixing of Atlantic-sourced waters (Wefing et al., 2021; Casacuberta and Smith, 2023; Payne et al., 2024).
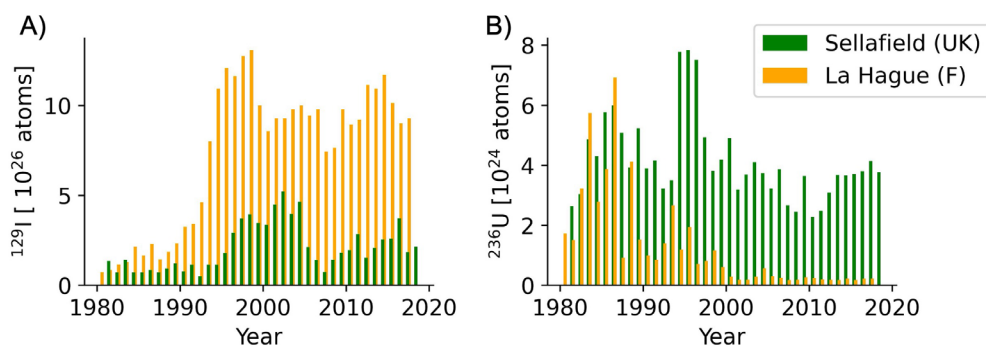

FIGURE 2
Annual discharge of **(A)** ^{129}I and **(B)** ^{236}U from the nuclear fuel reprocessing plants in Sellafield, United Kingdom (UK) and La Hague, France (F).

1.3 ^{129}I and ^{236}U in the subpolar North Atlantic

In the SPNA, ^{129}I proved to be a powerful tracer, especially in understanding the pathways and transport timescales of overflow waters such as DSOW, where it was observed since 1981 (Edmonds et al., 1998; Smith, 2005). Recent works by Castrillejo et al. (2018) and Dale et al. (2024) show that elevated concentrations of ^{129}I and ^{236}U are now highlighting the pathways of ISOW and LSW in the SPNA. The first dataset including both tracers took place along section A25 (or OVIDE line) in 2014 (Castrillejo et al., 2018) and two years later at Fram Strait (Wefing et al., 2019). These studies showed that Arctic Atlantic waters exiting the Fram Strait contained high tracer concentrations (up to ^{129}I: 645 ± 16 × 10^7 at/L, ^{236}U: 21.2 ± 0.5 × 10^6 at/L) (Wefing et al., 2019) within surface waters carried by the East Greenland Current (EGC) along the Greenland shelf. These waters are transported downstream to Irminger Sea (Havik et al., 2017; Holliday et al., 2007b), where concentrations of ^{129}I: 256 ± 4 × 10^7 at/kg, ^{236}U: 16 ± 2×10^6 at/kg were reported by Castrillejo et al. (2018) and Casacuberta and Smith (2023). In contrast to the high-latitude tracer-labeled water masses is the NAC which mostly brings the signal of global fallout from low latitudes (e.g., ^{129}I: 0.2–8×10^7 at/kg) (Castrillejo et al., 2018). Finally, the North East Atlantic Bottom Waters (NEABW) present in the Western European Basin carry almost no tracers. NEABW originates from the Southern Ocean and has not been exposed to anthropogenic sources of ^{129}I and ^{236}U. These high ranges of concentrations observed in the different water masses at SPNA are key to provide insights into ocean circulation between the Arctic Ocean and SPNA—for example, a very recent work by Dale et al. (2024) proved that the combination of ^{129}I and ^{236}U, in a binary mixing model, can be used to understand ocean circulation and mixing in the vicinity of Iceland. One of the key points of their work is that ISOW and DSOW have different tracer signatures, and thus ^{129}I and ^{236}U can be used to distinguish these two water masses downstream of their source regions.

This study aims to explore water mass provenance and mixing in the SPNA using ^{129}I and ^{236}U. To this end, new ^{129}I and ^{236}U data are presented in seawater collected in the Labrador Sea (2020) and on A25 section (2021). The new tracer data are related to water mass structure and circulation patterns. Provenance and mixing of water masses are then investigated using a ^{129}I–^{236}U binary mixing model. The ultimate goal of this work is to evaluate the strengths and limitations of the binary mixing model at this region of the SPNA.

2 Methods

2.1 Study area

This study focuses on two hydrographic transects represented by red squares in Figure 1. The transect A25 from Portugal to Cape Farewell in southern Greenland covered the OVIDE line. AR7W crosses the Labrador Sea from Hamilton Bank on the Labrador Shelf to Cape Desolation on the Greenland Shelf. A25 and AR7W

thus include four major basins, from east to west: the West European Basin (WEB), the Icelandic Basin, the Irminger Sea, and the Labrador Sea. The sections are suitably located to track water exchanges between the low-latitude Atlantic Ocean, Nordic, and Arctic seas. The major water masses and mean circulation of the SPNA are thoroughly reviewed in Daniault et al. (2016) and Liu and Tanhua (2021). Here the most important circulation features are briefly introduced in Figure 1 to provide the basis for the discussion of radionuclide distributions in Section 4.1. The WEB is mainly occupied by northward-flowing shallow waters originating from the subtropical gyre such as the East North Atlantic Central Water (ENACW), underlying Mediterranean Outflow Water (MOW), and a mixture of deep waters with a dominating influence from the Southern Ocean. In this work, deep waters bathing the WEB are named North East Atlantic Bottom Water (NEABW) following Liu and Tanhua (2021). To the west of the sub-Arctic front (≈22.5° W), low-latitude waters diminish to give way to higher-latitude waters. These include shallow waters with lower salinity such as the Subpolar Mode Water (SPMW) and intermediate waters such as LSW that may occupy the water column down to a maximum depth of 2000 m. Below that depth in the Labrador Sea and Iceland basin, dense overflows (ISOW, DSOW) are present after they overspill through sills between Iceland and either Greenland or Scotland, following primarily boundary currents at the Irminger and Labrador seas. Adopting the naming in Yashayaev (2007), waters in the Irminger Sea and the Labrador Sea derived from largely modified ISOW are named hereinafter Northeast Atlantic Deep Water (NEADW). Finally, surface and intermediate polar waters following the Irminger Sea and Labrador Sea boundaries are transported by boundary currents such as the East and the West Greenland Current (EGC and WGC). The latter waters mix with the inflow from the Canadian Arctic Archipelago and are transported by the Labrador Current (Pacini and Pickart, 2022).

2.2 Sampling

Sampling on AR7W took place in May 2020 onboard R/V Amundsen. A25 was visited in June 2021 onboard R/V Sarmiento de Gamboa during the BOCATS2 expedition. The fieldwork aimed at re-visiting stations that were previously sampled for ^{129}I and ^{236}U and to improve the spatial sampling resolution of ^{129}I from previous years. At A25, a total of 280 seawater samples (250 for ^{129}I and 30 for ^{236}U) from 18 depth profiles were collected, covering the WEB (Figure 1, stations 1 to 43), the Iceland basin (stations 44 to 66), the Reykjanes Ridge (stations 67 to 69), and the Irminger Sea (stations 70 to 91). At AR7W in the Labrador Sea, a total of five depth profiles (stations 92 to 110) and 98 seawater samples were collected (79 for ^{129}I and 19 for ^{236}U). The waters were sampled using a rosette equipped with 24 Niskin bottles and conductivity–temperature–depth sensors. The seawater samples for ^{129}I (250 mL) and ^{236}U (2–5 L) were stored in opaque bottles and plastic cubitainers, respectively. The sampling resolution of ^{236}U was lower than for ^{129}I due to water volume constraints. The samples collected on AR7W were shipped to the Laboratory of Ion Beam Physics (LIP) at

ETH-Zurich for chemical processing and analysis. On A25, the chemistry for iodine and partly for uranium was done onboard and finalized at LIP.

2.3 Sample processing and measurement

The sample processing for ^{129}I followed the method described elsewhere (e.g., Wefing et al., 2019) which was adapted originally from Michel et al. (2012). Briefly, sample aliquots of about 250 mL were spiked with about 1.5 mg of Woodward iodine (^{127}I) dissolved in solution. After thorough mixing, the aliquots were oxidized to iodate using saturated $Ca(ClO)_2$ solution and then reduced to iodide using $Na_2S_2O_5$ and $NH_2OH*HCl$. The reaction mixture was raised to pH 5 to pH 6 before passing through a preconditioned DOWEX 1 × 8 ion exchange resin to purify and retain the iodine. Then, 2.25 M KNO_3 was used to elute the iodine into an acidified $AgNO_3$ solution, and it was precipitated as AgI. The precipitate was dried, mixed with Ag powder, and pressed into cathodes for AMS measurements.

The compact 0.5-MV Tandy AMS facility at LIP was used to measure the atomic ^{129}I/^{127}I ratios which were normalized to two ETH-Zurich in-house standards with nominal ratios of ^{129}I/^{127}I = 38.995 ± 0.467 × 10^{-12} ("C2conc") and ^{129}I/^{127}I = 5.055 ± 0.068 × 10^{-12} ("C2dil"). The ^{129}I concentration in seawater was calculated based on the measured ^{129}I/^{127}I ratio and the known amount of added Woodward Iodine carrier (Vockenhuber et al., 2015; Christl et al., 2013).

To check for the analytical background and internal reproducibility, one blank and one internal seawater standard were included in every second batch of samples. The blank was prepared with deionized water ($n = 27$, ^{129}I = 3.8 ± 3 × 10^4 at/kg). The internal seawater standard was taken from station 15 on A25 ($n = 13$, ^{129}I = 11.88 ± 0.03 × 10^7 at/kg).

The seawater samples for ^{236}U were processed following the method described in Wefing et al. (2019) which consists of a pre-concentration and purification step. Briefly, the seawater samples of 2–5 L were acidified using concentrated HNO_3 (25%) and spiked with 1 pg of ^{233}U (acidic solution, PTB 2014-1126). Then, $Fe(NO_3)_2$ solution was added to the sample and precipitated as Fe_2O_3 using a concentrated NH_3 solution. The Fe_2O_3 precipitate was redissolved in 8 M HNO_3 and passed through UTEVA columns to purify U. The purified U was eluted, co-precipitated with Fe_2O_3, and thermally oxidized to UO. Finally, the precipitate was mixed with Nb powder and pressed into AMS cathodes.

The uranium isotopic ratios (^{236}U/^{238}U and ^{236}U/^{233}U) were analyzed using the compact AMS MILEA facility at LIP; details on the measurements are described by Christl et al. (2023). The measured ratios were normalized to the in-house ZUTRI ETH standard with a nominal isotopic ratio of 4055 ± 203 × 10^{-12} for ^{236}U/^{238}U and 3170 ± 830 × 10^{-12} for ^{233}U/^{238}U (Christl et al., 2013). The concentration of ^{236}U in the seawater samples was calculated using the isotopic ratios and the known amount of ^{233}U added to the sample. To correct for ^{236}U, the ^{236}U/^{233}U ratio was measured in chemistry blanks prepared with deionized water that was treated following the same procedure as that for the samples.

The blanks resulted in atom ratios of 5.75 ± 1.3 × 10^5 ($n = 2$) and 1.04 ± 0.08 × 10^4 ($n = 3$) for A25 and AR7W, respectively.

2.4 Data interpretation

Prior to the tracer analysis, water masses were defined using potential temperature and salinity following the work of García-Ibáñez et al. (2018) and Liu and Tanhua (2021).

The mixing of different water masses was studied using a binary mixing model based on two radionuclide tracers, namely, ^{129}I and ^{236}U. The key components of this 2D model are the endmembers, which represent the tracer signatures of specific water masses. These signatures are measured either at the water mass' source region or at a representative location where data is available. The endmembers create the boundary conditions that span between water masses with high tracer concentrations to others with low concentrations. All samples should fall within these boundary conditions, and the samples' tracer concentration is the result of the mixing between two different endmembers. This model has been previously described by Dale et al. (2024). In this work, we have extended the tracer space to other water masses found in the study region. The endmember locations are indicated by the triangles in Figure 1, and their location in the tracer space of the binary mixing model is shown in Figure 3. The error bars of each endmember represent the variability in the tracer concentrations within one water mass. An
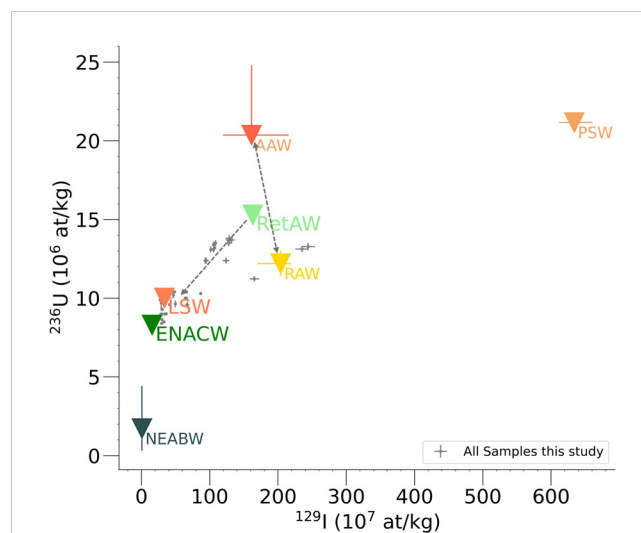

FIGURE 3
Overview of tracer data and water mass endmembers in a binary mixing model of ^{129}I–^{236}U. This study's samples are represented by gray symbols, while endmembers are shown in color with error bars indicating their maximum spread. Gray arrows illustrate the formation of RetAW by mixing AAW with RAW and a further dilution of IW (Dale et al., 2024), not shown here, which would be located at the ENACW endmember. The sampling year and references for the endmembers are provided in Supplementary Table S1, and their sampling location can be found in Figure 1. The LSW endmember is derived from samples in this study; its sampling location is indicated in Figure 4. AAW, Arctic Atlantic Water; ENACW, Eastern North Atlantic Central Water; LSW, Labrador Sea Water; NEABW, North East Atlantic Bottom Water; PSW, Polar Surface Water; RAW, Recirculating Atlantic Water; RetAW, Return Atlantic Water.

overview of the mean, minimum, and maximum tracer concentrations as well as the corresponding hydrographic properties is given in Supplementary Table S1. The endmember tracer values adopted here were mostly assigned in earlier works (Castrillejo et al., 2022, 2018; Wefing et al., 2019; Dale et al., 2024).

In the SPNA, the endmembers (Figure 3) with the highest tracer concentrations are the water masses with the direct influence of European nuclear reprocessing plants (Casacuberta and Smith, 2023). These waters, namely, Arctic Atlantic Water (AAW, red triangle, Figure 3) and polar surface water (PSW, orange triangle), recirculated in the Arctic Ocean and entered the SPNA as the East Greenland Current (EGC) was exiting the Arctic Ocean via Fram Strait and passing the Nordic Seas (Holliday et al., 2007b; Vage et al., 2013). A third water mass, the Return Atlantic Water (RetAW, light green triangles), is formed by the mixing of Arctic Atlantic Water (AAW) with Recirculating Atlantic Water (RAW) (Dale et al., 2024) and RAC (Wefing et al., 2022, 2019) which did not enter into the Arctic Ocean (Dale et al., 2024; Wefing et al., 2019, 2022; De Steur et al., 2014; Olsson et al., 2005; Rudels, 2002). In contrast, ENACW (teal triangle) provides the best estimate for waters coming from upstream locations relative to nuclear reprocessing plants and thus carries relatively low concentrations of both ^{129}I and ^{236}U mostly derived from nuclear weapon tests (Castrillejo et al., 2018).

The endmembers of AAW and PSW correspond to values observed in Fram Strait in 2016 (Wefing et al., 2019). Although Fram Strait was sampled in 2018 and 2019, we decided to choose the 2016 data because of its stronger influence on the Arctic Atlantic outflowing water (Wefing et al., 2022), and it already proved to be a suitable endmember for the upstream water mass formation (Dale et al., 2024). The RetAW is represented by values obtained from the GEOTRACES Metal Gate cruise and monitoring program around Iceland in 2021 and represents the best estimate of the high tracer concentration in water masses originating in the Nordic Seas (Dale et al., 2024). The ENACW and NEABW endmembers were classified after Castrillejo et al. (2018). An average of all tracer measurements was calculated for NEABW. On the other hand, measurements at their GEOVIDE Station 26 (50°16.67′ N, 22°36.28′ W) were found to best represent the reprocessing-free waters carried by the NAC.

The water mass fraction is calculated by dividing the distance between the sample and one endmember by the total distance between the two endmembers. For each water mass, this model considers the mixing between two endmembers only, which is one of its main limitations. However, the tracer signature in each water mass is only affected by mixing with tracer-labeled water masses and is not subject to hydrographic changes. This allows one to quantify mixing in a 2D model between tracer-rich Arctic-origin water and tracer-poor water of Atlantic origin. Currently, the model reaches its limitations, where the overall tracer concentration is low (^{129}I: 20–50 × 10^7 at/kg; ^{236}U: 8.5–10.5×10^6 at/kg) and the tracer input happens via multiple vertical and lateral mixing processes and sources. This might be addressed by including the tracers in an optimum multiparameter analysis (Poole and Tomczak, 1999), which is not the scope of this manuscript but could be achieved in future studies as more data become available.

3 Results

All radionuclide data are reported in atoms per kilogram (at/kg) along with metadata and hydrographic variables (T, S) in Supplementary Table S2, while the acronyms are listed in Appendix A. The concentrations of ^{129}I with overlaid salinity and ^{236}U concentrations are presented in Figure 4. The distributions of ^{129}I and ^{236}U are related to the water masses of the region following the classifications and naming from García-Ibáñez et al. (2018) and Liu and Tanhua (2021) and earlier work on these tracers in the SPNA (Castrillejo et al., 2022, 2018).

The geographical distribution of ^{129}I (Figure 4A) shows increasing concentrations from east to west. The lowest ^{129}I concentrations, ≈ 0.2 × 10^7 at/kg, were found below 3000 m in the WEB. The highest ^{129}I concentrations, up to 235 × 10^7 at/kg, were observed in surface waters in the Labrador and Irminger seas. Intermediate concentrations, between 30 and 40 × 10^7 at/kg, were found at intermediate depths between the Iceland Basin and the Labrador Sea. The fewer ^{236}U data (Figure 4B) generally followed the distribution of ^{129}I. As for ^{129}I, ^{236}U was highest at shallow depths in the vicinity of Greenland and near-bottom depths of the Labrador Sea and Irminger Sea (>13 × 10^6 at/kg, >2700 m). The average concentrations of ^{236}U (9 to 10 × 10^6 at/kg) corresponded to intermediate depths in these basins, while lower concentrations (<9 × 10^6 at/kg) filled the bottom depths east of Reykjanes Ridge.

In the WEB, depths greater than 3000 m were occupied by cold and relatively fresh (T_{pot}< 2.6°C, S < 34.90,^{129}I: <1 × 10^7 at/kg) northward-flowing NEABW. At about 1000 m depth was the core of the saline and warm MOW (T_{pot}≈ 11.7°C, S > 36.00, ^{129}I: 5–7 × 10^7 at/kg), more concentrated near Portugal. The shallower depth layer was filled by the warmer ENACW with elevated ^{129}I (T_{pot}> 12° C, S: 35.4–35.7, ^{129}I: 5-14 × 10^7 at/kg).

The upper 700 m in the Iceland Basin was occupied by comparable fresher and colder Subpolar Mode Water (SPMW, T_{pot}: 7.2°C, S: 35.07) and SAIW (T_{pot}: 6.0°C, S: 34.7) that contained ^{129}I concentrations between 20 × 10^7 and 35 × 10^7 at/kg. Below SPMWs was LSW (T_{pot}: ≈3°C, ^{129}I: 30 × 10^7 at/kg) with comparable salinity but colder temperature. Confined to the eastern flank of the Reykjanes Ridge was ISOW (T_{pot} ≈ 3.5°C, S ≈ 34.95, ^{129}I: 41 × 10^7 at/kg), while the NEADW (T_{pot} ≈ 2.9°C, S ≈ 34.92, ^{129}I: 27–48 × 10^7 at/kg) was occupying a similar depth in the Irminger and Labrador seas.

In the Labrador and Irminger seas, near-bottom depths were filled by the very dense, cold, and fresher DSOW (T_{pot}<1.5°C, S < 34.92) that contained high ^{129}I concentrations between 108.6 ± 1.3 × 10^7 at/kg and 131.6 ± 5.4 × 10^7 at/kg. The remaining water column structure in the Labrador Sea largely resembled that of the Irminger Sea. The cold and freshest water mass in both basins, the Polar Surface Water (S < 34.92), was carried along the Greenland and Canada shelves by the Western Boundary Current as part of the EGC, the WGC, and the Labrador Current. The highest ^{129}I concentration up to 235 × 10^7 at/kg, measured in this study, characterized the EGC and WGC at the Greenlandic shelf. The Labrador Current also showed elevated ^{129}I (95 × 10^6 at/kg), although not as high as in the EGC. The surface waters in the
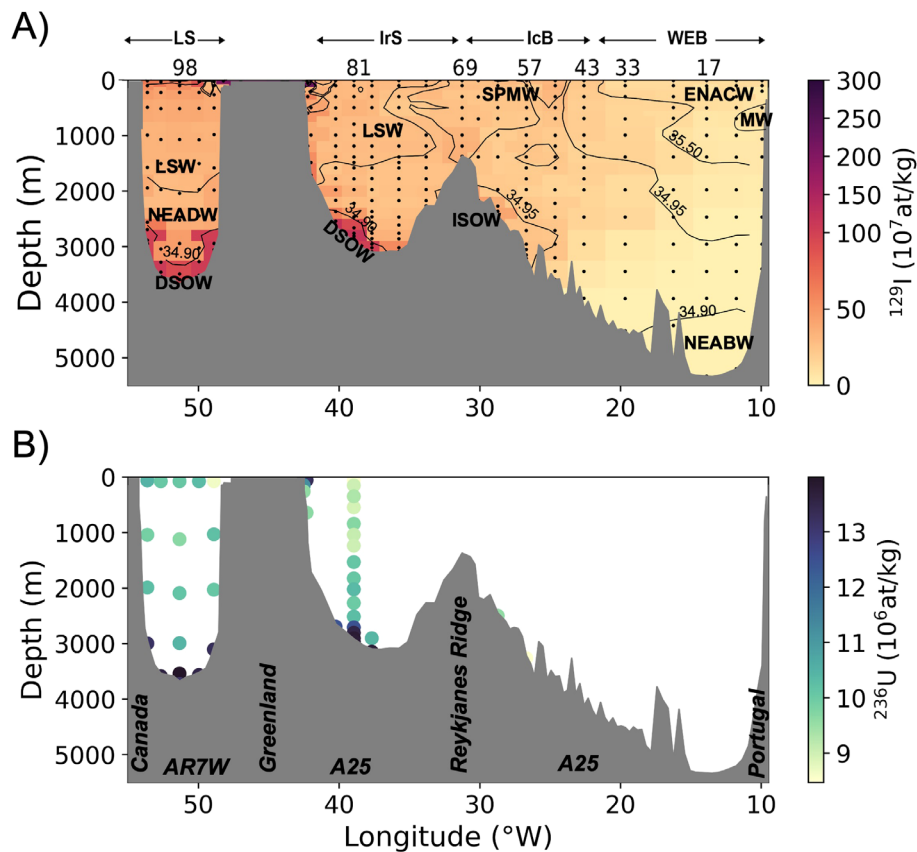
FIGURE 4
Zonal distribution of **(A)** ^{129}I and **(B)** ^{236}U concentrations along A25 and AR7W, respectively, in 2021 and 2020. Isohalines (black lines) overlay the interpolated ^{129}I concentrations to represent the water mass distribution following Daniault et al. (2016); Liu and Tanhua (2021), and Yashayaev (2007). The ^{236}U concentrations, fewer in number, are represented as colored dots.

middle of the Labrador Sea showed a heterogeneous distribution with ^{129}I in the range of 30–60 $\times$ 10^7 at/kg.

The ^{236}U distribution was detailed for the Labrador Sea but limited to one full-depth station in the central Irminger Sea and a few other samples within the Irminger Sea and east of Reykjanes Ridge. The ^{236}U distribution in the Labrador and Irminger seas (Figure 4B) was similar to ^{129}I but displayed a narrower range of concentrations: 8.4 to 14 $\times$ 10^6 at/kg. The highest ^{236}U concentrations were located in the EGC (13.1 $\pm$ 0.2 $\times$ 10^6 at/kg) and DSOW (13.8 $\pm$ 0.2 $\times$ 10^6 at/kg). Then declined to 10.4 $\times$ 10^6 at/kg in the NEADW and LSW and to 8.6 $\pm$ 0.2 $\times$ 10^6 at/kg in the SPMW.

4 Discussion

The distribution of ^{129}I and ^{236}U in the SPNA varies over time and space due to two primary factors: discharges from nuclear reprocessing plants and changes in ocean circulation. Nuclear reprocessing plants have been releasing ^{129}I and ^{236}U since the 1960s, but their contributions to the North Sea have fluctuated. ^{236}U discharges peaked in the 1980s, while ^{129}I discharges increased exponentially between 1990 and 2000 (Figure 2) (Casacuberta and Smith, 2023). The circulation and mixing of water masses transport distinct tracer signals based on their origin and mixing processes. If

ocean circulation is unchanging, the circulation should reflect the dynamics of nuclear reprocessing plant discharges. However, this relationship may be disrupted if circulation patterns and, consequently, mixing change.

To disentangle the two drivers of ^{129}I and ^{236}U concentrations in the SPNA, firstly, we relate the distribution of both tracers to the circulation patterns in 2020/2021. Secondly, we examine the potential of using ^{129}I and ^{236}U in a binary mixing model that allows us to understand water mass provenance and mixing in the SPNA.

4.1 Tracer distribution in relation to circulation patterns

To relate the tracer distribution to the circulation patterns, both ^{129}I and ^{236}U are plotted in iso-surface maps at the surface (upper 50 m), intermediate (1,500 m/1,000 m), and bottom depths (deepest sample). Due to scarcity of ^{236}U, the discussion mainly focuses on the ^{129}I distribution. At the surface (Figures 5A, B), the highest concentrations of both tracers are observed in the East/West Greenland currents both in the Irminger Sea (^{129}I: 235.2 $\pm$ 9.8 $\times$ 10^7 at/kg) and Labrador Sea (^{129}I: 232.0 $\pm$ 2.8 $\times$ 10^7 at/kg). These high concentrations relate to the ones observed at East Greenland Current (EGC) both in Fram Strait (^{129}I: 645 $\pm$ 2.1 $\times$ 10^7 at/kg) and downstream
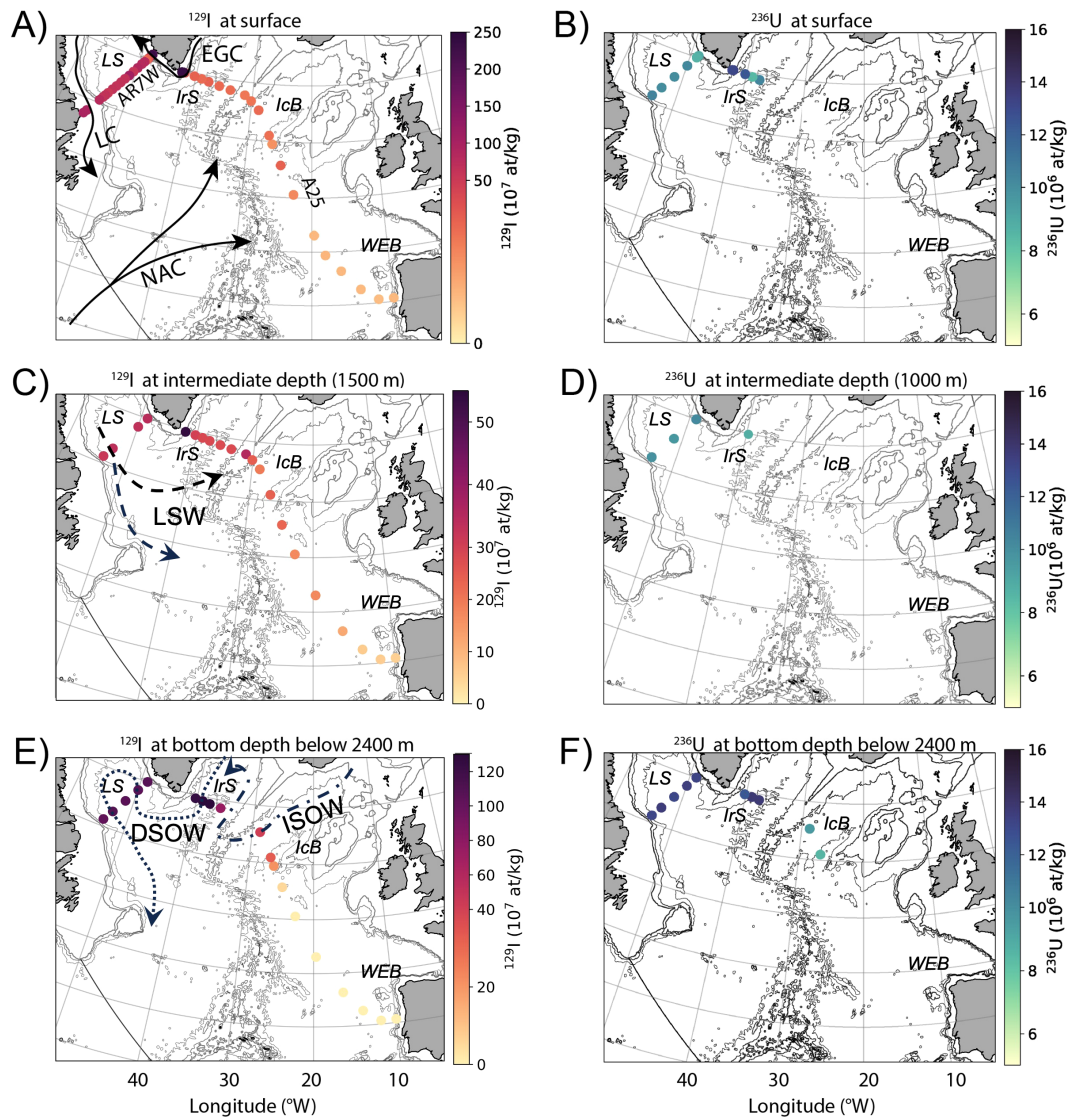
FIGURE 5
Isosurface distributions of ^{129}I and ^{236}U concentrations at **(A, B)** the surface, **(C)** 1,500 m for ^{129}I, **(D)** 1,000 m for ^{236}U, and **(E, F)** bottom depth below 2,400 m.

at Denmark Strait (^{129}I: 432 ± 21.7 ×10^7 at/kg) (Wefing et al., 2019; Dale et al., 2024), indicating the advectiveness of this current from its source region in Fram Strait down to the tip of Greenland. The ^{129}I content of the Labrador Current (95 × 10^7 at/kg) is about half of the concentrations observed in the EGC (235 × 10^7 at/kg), most probably being related to a mixing of the West Greenland Current (WGC) with ^{129}I-poor Arctic waters carried by the Baffin Iceland Current. These waters enter the Labrador Sea through the Arctic–Canadian Archipelago and mix at the Davis Strait (Wefing et al., 2022; Pacini and Pickart, 2022; Chamizo et al., 2022). The heterogeneous tracer distribution in the central Labrador Sea (Figure 5A) might reflect the eddy transport of tracer-rich polar surface water (PSW) from the boundary current to the open ocean (Holliday et al., 2020; Lilly et al., 2003; Gou et al., 2022; Holliday et al., 2007b). Moving to the east of the A25 line, surface tracer concentrations progressively decrease to 10 × 10^7 at/kg.

This highlights the subarctic front at 22.5°W with a sudden drop (station 50, ^{129}I: 34.3 ± 1.4 × 10^7 at/kg to station 43, ^{129}I: 23.1 ± 1 × 10^7 at/kg) in the tracer concentration. The lowest values (<2.5 × 10^7 at/kg) at the surface never reach values as low as the ones expected from global fallout (Edmonds et al., 1998; Castrillejo et al., 2018). This is in agreement with previous studies that suggest the formation of Eastern North Atlantic Central Water (ENACW) as a result of mixing between Subpolar Mode Water (SPWM, tracer-labeled) and tracer-poor, nuclear reprocessing plant-free tropical waters transported by the North Atlantic Current (NAC) (Liu and Tanhua, 2021; Castrillejo et al., 2022; Daniault et al., 2016). This interpretation differs from He et al. (2013) and Castrillejo et al. (2017) who suggested a direct influence of the nuclear reprocessing plants by waters approaching from France and the UK toward the coast of Portugal and from the MW which still carries the imprint from the closed nuclear reprocessing plant of Marcoule in Southern

France. However, the gradual decrease in surface concentration from west to east might favor the influence of SPMW on ENACW.

At intermediate depths, the highest concentrations of both tracers were observed at the Labrador and Irminger seas (Figures 5C, D). One of the hypotheses is that the tracers remain at this depth due to winter convection and/or re-circulation within the subpolar gyre. This finding is consistent with previous studies tracking the re-circulation and pathways of Labrador Sea Water (LSW) using hydrographic data, ARGO floats, CFCs, and ^{129}I (Holliday et al., 2007a, 2009; Rhein et al., 2011; Castrillejo et al., 2022). Another explanation is that tracer concentrations at intermediate depths are coming from upstream locations, e.g., at mid-depths at Denmark Strait (Rudels, 2002), something that will be further discussed with the binary-mixing model in Section 4.3. Toward the east, the concentrations gradually decrease, showing the influence of LSW at intermediate waters and at least as far as 32.5°W. LSW are mostly formed in the middle of the Labrador and Irminger seas, thus having ^{129}I and ^{236}U concentrations that are further diluted from the ones observed at the surface of the Labrador Sea (^{129}I $< 50 \times 10^7$ at/kg).

Below 2400 m (Figures 5E, F), a clear separation is observed between tracer-rich waters west and along the flanks of the Reykjanes Ridge and tracer-poor waters at the eastern part of the transect. In agreement with previous studies (Smith, 2005; Castrillejo et al., 2022), the high tracer concentrations are carried by the two overflow waters: Denmark Strait Overflow Water (DSOW) and Iceland Scotland Overflow Water (ISOW). These two water masses overflowing through the Greenland–Iceland and Iceland–Scotland passages pick the tracer signal from shallower depths and bring it to the abyssal layers (Dale et al., 2024). On the contrary, the deep North East Atlantic Bottom Water (NEABW) from the south carries the natural ^{129}I signal, thus representing very old waters that have not yet seen the anthropogenic influence of neither weapon test nor reprocessing plant discharges.

4.2 Pseudo-steady-state of the tracers in the study area

The discharges of both ^{129}I and ^{236}U into the marine environment have varied over time (Figure 2), allowing for their use as transient tracers, thereby requiring a non-steady state approach (Casacuberta and Smith, 2023; Payne et al., 2024). In this study, however, we follow the approach described in Dale et al. (2024) where the tracers are assumed to be not significantly changing during the period from 2016 till the present. The study of Dale et al. (2024) proves that while the tracer signature of the Atlantic water entering the Arctic Ocean is changing over time, the rate of change of the inputs is slow enough that one can compare the measurements of water masses relatively proximal in the ocean circulatory system. Small changes in the inputs and upstream mixing regimes are represented by error bars of the endmembers (Figure 3), showing the maximal spread of tracer concentration within one source water mass. In comparison, the error bars attached to the samples of this study represent the analytical error which is significantly smaller. Here the validity of this assumption is further addressed by looking at the time variability of tracer

concentrations in water masses sampled in previous years. Figure 6 shows the ^{129}I vs. ^{236}U concentrations from 2014 (GEOVIDE, light gray) (Castrillejo et al., 2018), 2018 (OVIDE, dark gray) (Castrillejo et al., 2022), and 2020/2021 (this study, blue), where deep and intermediate water masses cluster at two different domains within the ^{129}I –^{236}U tracer space. The cluster that plots on the top right represents the core of DSOW, while the cluster plotting at the bottom left represents the intermediate waters, both in the Irminger and Labrador seas. When looking at the DSOW cluster of the Irminger Sea (blue diamonds), there are slight differences in ^{129}I and^{236}U concentrations between the years 2018 and 2021 (no data for 2014), with more recent data located at higher ^{129}I. The observed increase in ^{129}I corresponded well with further releases in ^{129}I after 1999 (Figure 2), with transit times of 16–18 years from the North Sea to the deep Irminger and Labrador seas (Castrillejo et al., 2018) and about 1 year from Denmark Strait sill to Cape Farewell (Xu et al., 2015). The DSOW cluster sampled in the Labrador Sea (blue crosses) overlaps the DSOW sampled in the Irminger Sea in 2018 (gray diamonds) which showed the advective character and a transit time of about 1 year, which is in agreement with earlier studies (Xu et al., 2015; Smith, 2005). The concentrations of both tracers could indeed have been different for both years considering the discharge history. However, the DSOW samples from 2018 and 2021 in Figure 6 remain very clustered and detached from the rest considering the strong mixing in the Nordic Seas, which points toward a diffusive formation and thus a dilution of the tracer signal along the formation pathway. This proves the robustness of the binary mixing model (Figure 3) and validates the assumption of a steady state.

4.3 Water mass provenance and mixing

To study the provenance and mixing of water masses, we utilized the binary mixing model described in Section 2.4. Since this model relies on the concentration of both ^{129}I and ^{236}U, the discussion is limited to data that includes both tracers. Water masses were assigned using hydrographic data, as described in Section 3 . Results and the Supplementary Material.

The surface samples (Figure 7A, blue diamonds) with the highest concentrations of both ^{129}I and ^{236}U are located in the Irminger Sea and sampled within the EGC. They are a further dilution of station MG17 (Dale et al., 2024) sampled north of Denmark Strait and nicely show the continuation of the EGC along the Greenlandic Coast. The samples of this study were taken during the transit from the central Irminger Basin to the coast of Greenland. Thus, samples that plot closer to the PSW endmember correspond to the ones that best represent the core of the EGC. These waters preserve a significant fraction (i.e., 29%–32%) of the Polar Surface Water exiting the Arctic Ocean through the Fram Strait. The samples that plot down the mixing line indicate the mixing with the low-tracer northward-flowing ENACW. This work therefore corroborates previous studies about the connection and evolution of the waters exiting the Arctic Ocean and being transported to lower latitudes through the EGC (Holliday et al., 2007b; Sutherland et al., 2009). However, while other studies relied on the use of hydrographic parameters and models only (Holliday et al., 2007b; Sutherland et al., 2009), this is
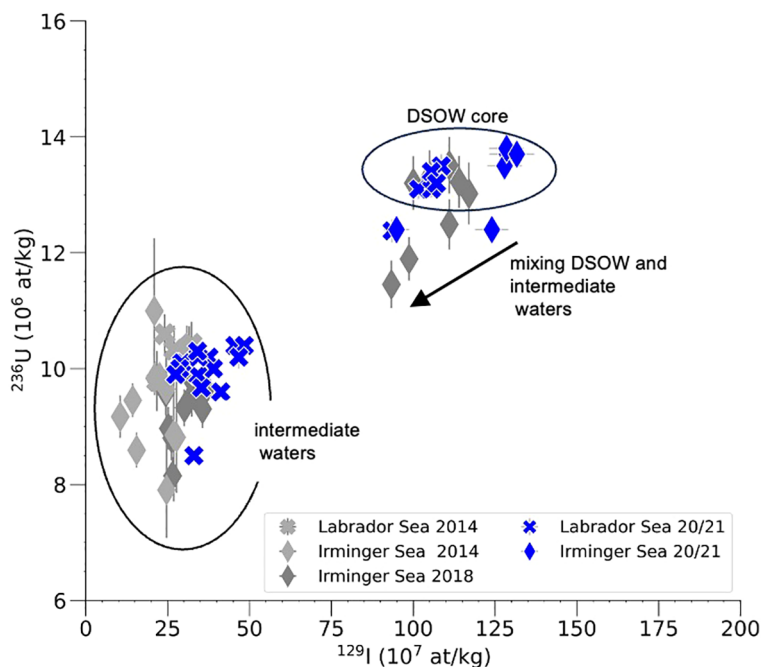
FIGURE 6
Historic evolution of the tracers in the ^{129}I–^{236}U binary mixing model between 2014 (light gray), 2018 (dark gray), and 2020/2021 (blue). The Labrador Sea was not sampled in 2018.

the first work that uses radionuclide tracers as a new tool to understand the contribution of PSW to the East and West Greenland currents and further to the formation of LSW.

The composition of the DSOW (Figure 7B, dark blue diamonds and crosses) in the Irminger and Labrador seas is mainly a mixture of Return Atlantic Water (RetAW) with LSW and North East Atlantic Deep Water (NEADW). Small fractions of strongly tracer-labeled waters such as PSW (orange triangle Figure 3, Supplementary Table S1) and AAW (red triangle Figure 3) may contribute to the formation of DSOW (Rudels, 2002; Dale et al., 2024; Tanhua et al., 2005; Tanhua, 2005; Lin et al., 2020), which could lead to the two observed DSOW clusters. The cluster plotting slightly left of the two endmembers' mixing line and with lower ^{129}I concentrations represents samples in the Labrador Sea with a fraction of RetAW of 20%–24%. The second cluster composed of samples in the Irminger Sea plots on top of the RetAW-LSW/NEADW mixing line with a fraction of RetAW of 27%–35%, which is in agreement with the 33%–43% reported by Dale et al. (2024). A stronger contribution of AAW to the formation of RetAW might already lead to an increase of ^{129}I with respect to the ^{236}U concentrations. A dilution of DSOW between the Irminger Sea and Labrador Sea is less likely (see Figure 6B) since the signal of DSOW found in 2018 in Irminger Sea is well conserved in the Labrador Sea signal in 2020, which agrees with a transit time of about 1 year (Xu et al., 2015; Tanhua, 2005). Another feature observed here is that once we move away from the DSOW core, the tracers show a strong influence of intermediate water masses such as NEADW/ISOW, which is in agreement with the observations of Dale et al. (2024) (Figure 7B, gray-shadowed circle).

At the southern part of the Reykjanes Ridge, ISOW (Figure 7C, yellow diamonds) is already entrained by 60% of LSW (Dale et al., 2024; Fogelqvist et al., 2003) and located at lower tracer concentrations. Johns et al. (2021) described two branches of ISOW on the eastern flank of Reykjanes Ridge that are visible in the tracer space: the main branch has higher ^{236}U and plots close to the NEADW cluster, representing the main influence of LSW and SPMW (Furey et al., 2024). The second branch might have a stronger influence of NEABW and therefore lower ^{236}U concentration, which is in agreement with the water mass analyzed by García-Ibáñez et al. (2015). However, since the data of the dual tracer pair in this region is limited, a further interpretation of the spatial distribution along the Reykjanes Ridge is not yet possible.

The evolution of ISOW to NEADW (brown crosses) from the Irminger Sea to the Labrador Sea can be followed by increasing ^{236}U and a slight increase in ^{129}I, which could be attributed to a further entrainment of LSW and mixing with DSOW (Dale et al., 2024; García-Ibáñez et al., 2015; Furey et al., 2024; Smethie et al., 2000; Stramma et al., 2004). As the mixing with DSOW seems to push the ISOW to a slightly higher ^{236}U, the NEADW, in turn, leads to a spread of DSOW to lower ^{236}U at the mixing interfaces.

Finally, LSW is generally very diluted with regard to both tracers and thus located at the lower end of the tracer space (Figure 7D). The LSW (orange diamonds and crosses) might have multiple tracer sources, as it is formed via vertical winter time convection, lateral mixing between intermediate waters in Labrador and Irminger seas, and advection of DSOW into bottom waters (Yashayaev, 2024; Xu et al., 2015; Dale et al., 2024). A tracer source to the surface are eddies emerging from the boundary currents (EGC/WGC, LC) to the central Labrador Sea (Zunino et al., 2017),
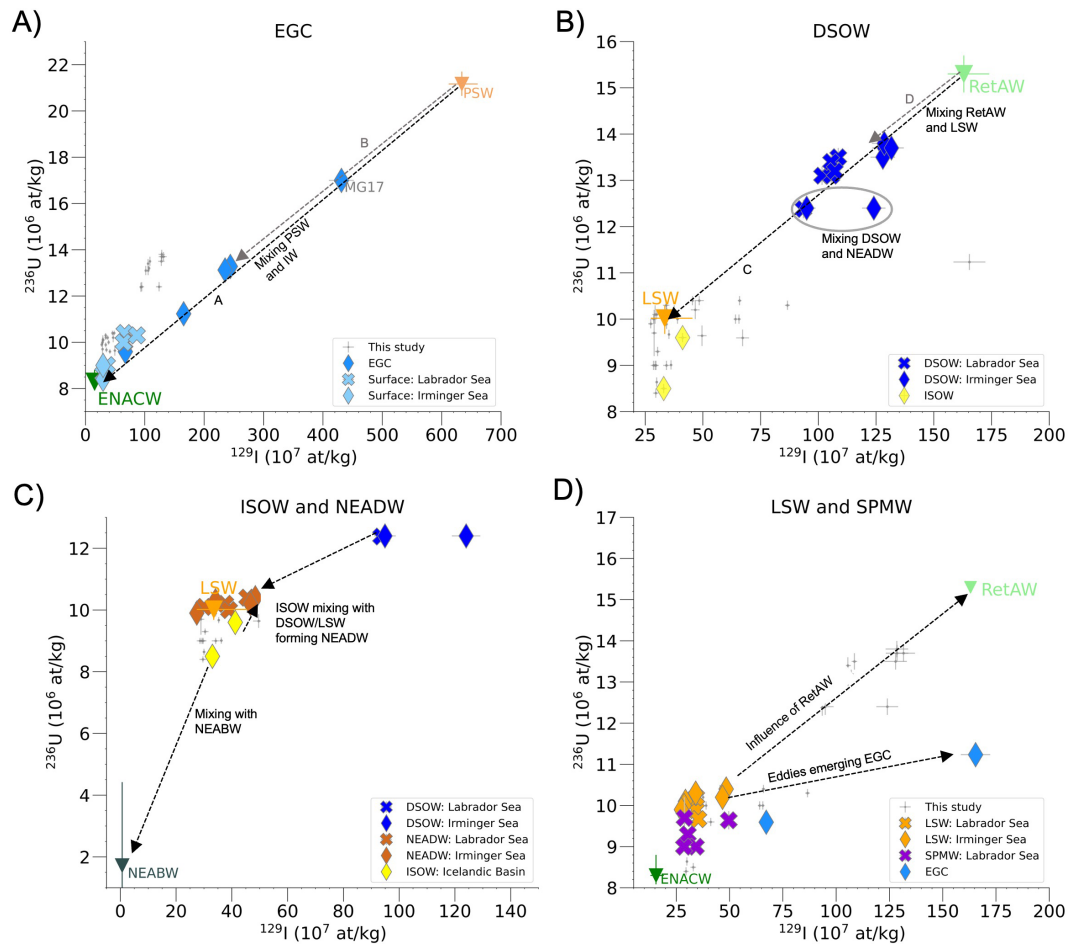
FIGURE 7
Binary mixing model of ^{129}I–^{236}U with endmembers as previously described in Figure 3. Gray symbols represent all study samples, while different colors highlight different water masses. **(A)** EGC and surface waters, with mixing calculated as: PSW (fraction) = length A/B, **(B)** DSOW and its formation by dilution of RetAW with LSW as calculated by fraction RetAW = length C/D, **(C)** ISOW and NEADW, and **(D)** LSW and SPMW. Triangles represent endmembers as described in Supplementary Table S1 and Figure 3, while the dotted lines indicate mixing between different water masses. All acronyms are detailed in Appendix A.

carrying especially high ^{129}I concentration. While eddies may contribute to the observed tracer concentrations during winter convection, they cannot be the sole source, as the tracer signature within the EGC is characterized by high levels of ^{129}I but relatively low levels of ^{236}U. The RetAW introduced to the LSW via passing over the Eastern Greenland continental shelf (Rudels et al., 1999; Pickart, 1992; Zou et al., 2024) and mixing across density surfaces seems to be another tracer source, considering the higher ^{236}U concentration in LSW located at Irminger Basin in comparison to the LSW located at Labrador Sea. This further supports the hypothesis of Dale et al. (2024) of a "contamination" of the intermediate waters at the subpolar gyre with elevated ^{236}U due to entrainment of RetAW. Furthermore, the recirculation of LSW within the subpolar gyre might cause a smoothing of the tracer signal and preserve higher ^{236}U concentrations in older waters (Lavender et al., 2005; Lozier et al., 2013). To further evaluate the tracer sources to the LSW, tracer pair data of the WGC, LC, and from the Davis Strait would be necessary (Wefing et al., 2021; Chamizo et al., 2022; Colombo et al., 2019; Zhang et al., 2021a, b).

Finally, the SPMW (purple crosses) plots at comparable low ^{236}U concentrations. This suggests the strong influence of eddies emerging from the EGC (Holliday et al., 2009).

5 Conclusion

This study aimed to constrain the origin and mixing of water masses in the subpolar North Atlantic by combining two artificial radionuclides, ^{129}I and ^{236}U. To that end, we used new data collected in the A25 (OVIDE) and AR7W (Labrador Sea) lines in 2020/2021 and used a new dual tracer approach to infer water mass provenance and mixing. The results for both radionuclides tracers, ^{129}I and ^{236}U, were consistent with tracer distributions reported in earlier studies but highlighted the contrast between high-tracer waters influenced by nuclear reprocessing plants and low-tracer waters originating from southern latitudes. Using the tracer pair in a binary mixing model, the PSW contributes 29–32% to the EGC at Cape Farewell. With 29%–35%, RetAW was found

to be a main contributor to DSOW in the Irminger and Labrador seas.

The binary mixing model reached its limitation in the identification of the water mass composition of LSW, SPMW, and ISOW because of the availability of suitable endmembers. A more detailed sampling of possible contributors was conducted in the Nordic Seas and Baffin Bay (2022). This will help constrain better endmembers to investigate the origin and mixing of these water masses. Overall, the study shows that ^{129}I and ^{236}U are suitable to address the provenance and mixing of key components of the SPNA circulation, which contributes to a better understanding of circulation patterns, pathways and mixing of water masses, and their effect on the evolution of the AMOC. While this study also points to the limitations of this method, it underscores the potential of ^{129}I and ^{236}U as valuable tracers to validate and improve ocean circulation models, particularly in the complex mixing zones of the North Atlantic.

Data availability statement

The original datasets for this study can be found in the article/ Supplementary Material and radioisotope data are available at MARIS (Marine Radioactivity Information System): https://maris. iaea.org/datasets. The CTD-Oxygen data from the OVIDE cruise are reported in Le Bihan et al. (2023).

Author contributions

LL: Writing – original draft, Visualization, Validation, Methodology, Formal analysis, Data curation. MCa: Writing – review & editing, Visualization, Validation, Supervision, Data curation. JS: Writing – review & editing. MCh: Writing – review & editing, Resources, Data curation. CV: Writing – review & editing, Data curation. AV: Data curation, Validation, Investigation, Funding acquisition, Resources, Writing – review & editing. PL: Data curation, Validation, Investigation, Funding acquisition, Resources, Writing – review & editing. NC: Writing – review & editing, Supervision, Resources, Project administration, Funding acquisition, Conceptualization.

Funding

Acknowledgments

Conflict of interest

The authors declare that the research was conducted in the absence of any commercial or financial relationships that could be construed as a potential conflict of interest.

Publisher's note

All claims expressed in this article are solely those of the authors and do not necessarily represent those of their affiliated organizations, or those of the publisher, the editors and the reviewers. Any product that may be evaluated in this article, or claim that may be made by its manufacturer, is not guaranteed or endorsed by the publisher.

Supplementary material

The Supplementary Material for this article can be found online at: https://www.frontiersin.org/articles/10.3389/fmars.2024.1470675/ full#supplementary-material

SUPPLEMENTARY TABLE 1
Hydrographic and tracer data for GEOVIDE.

SUPPLEMENTARY TABLE 2
Endmember concentration and hydrographic water mass properties.

SUPPLEMENTARY TABLE 3
Hydrographic and tracer data for A25 and AR7W.

References

Aldahan, A., Alfimov, V., and Possnert, G. (2007). ^{129}I anthropogenic budget: Major sources and sinks. *Appl. Geochemistry* 22, 606–618. doi: 10.1016/j.apgeochem.2006.12.006

Alfimov, V. (2004). Tracing water masses with ^{129}I in the western Nordic Seas in early spring 2002. *Geophysical Res. Lett.* 31, L19305. doi: 10.1029/2004GL020863

Bower, A., Lozier, S., Biastoch, A., Drouin, K., Foukal, N., Furey, H., et al. (2019). Lagrangian views of the pathways of the atlantic meridional overturning circulation. *J. Geophysical Research: Oceans* 124, 5313–5335. doi: 10.1029/ 2019JC015014

Bower, A. S., Lozier, M. S., Gary, S. F., and Böning, C. W. (2009). Interior pathways of the North Atlantic meridional overturning circulation. *Nature* 459, 243–247. doi: 10.1038/nature07979

Casacuberta, N., Christl, M., Vockenhuber, C., Wefing, A.-M., Wacker, L., Masqué, P., et al. (2018). Tracing the three atlantic branches entering the arctic ocean with ^{129}I and ^{236}U. *J. Geophysical Research: Oceans* 123, 6909–6921. doi: 10.1029/2018JC014168

Casacuberta, N., Masqué, P., Henderson, G., Rutgers van-der Loeff, M., Bauch, D., Vockenhuber, C., et al. (2016). First ^{236}U data from the Arctic Ocean and use of ^{236}U/^{238}U and ^{129}I/^{236}U as a new dual tracer. *Earth Planetary Sci. Lett.* 440, 127–134. doi: 10.1016/j.epsl.2016.02.020

Casacuberta, N., and Smith, J. N. (2023). Nuclear reprocessing tracers illuminate flow features and connectivity between the arctic and subpolar north atlantic oceans. *Annu. Rev. Mar. Sci.* 15, 203–221. doi: 10.1146/annurev-marine-032122-112413

Castrillejo, M., Casacuberta, N., Christl, M., Garcia-Orellana, J., Vockenhuber, C., Synal, H.-A., et al. (2017). Anthropogenic ^{236}U and ^{129}I in the Mediterranean Sea: First comprehensive distribution and constrain of their sources. *Sci. Total Environ.* 593-594, 745–759. doi: 10.1016/j.scitotenv.2017.03.201

Castrillejo, M., Casacuberta, N., Christl, M., Vockenhuber, C., Synal, H.-A., García-Ibáñez, M. I., et al. (2018). Tracing water masses with \textbackslashchem^129I and \textbackslashchem^236U in the subpolar North Atlantic along the GEOTRACES GA01 section. *Biogeosciences* 15, 5545–5564. doi: 10.5194/bg-15-5545-2018

Castrillejo, M., Casacuberta, N., Vockenhuber, C., and Lherminier, P. (2022). Rapidly increasing artificial iodine highlights pathways of Iceland-scotland overflow water and labrador sea water. *Front. Mar. Sci.* 9. doi: 10.3389/fmars.2022.897729

Chamizo, E., Christl, M., López-Lora, M., Casacuberta, N., Wefing, A., and Kenna, T. (2022). The potential of ^{233}U/^{236}U as a water mass tracer in the arctic ocean. *C. J. Geophysical Research: Oceans* 127, e2021JC017790. doi: 10.1029/2021JC017790

Christl, M., Casacuberta, N., Lachner, J., Maxeiner, S., Vockenhuber, C., Synal, H.-A., et al. (2015a). Status of ^{236}U analyses at ETH Zurich and the distribution of ^{236}U and ^{129}I in the North Sea in 2009. *Nucl. Instruments Methods Phys. Res. Section B: Beam Interact. Materials Atoms* 361, 510–516. doi: 10.1016/j.nimb.2015.01.005

Christl, M., Casacuberta, N., Vockenhuber, C., Elsässer, C., Bailly du Bois, P., Herrmann, J., et al. (2015b). Reconstruction of the ^{236}U input function for the northeast atlantic ocean: Implications for ^{129}I/^{236}U and ^{236}U/^{238}U-based tracer ages. *J. Geophysical Research: Oceans* 120, 7282–7299. doi: 10.1002/2015JC011116

Christl, M., Gautschi, P., Maxeiner, S., Müller, A. M., Vockenhuber, C., and Synal, H.-A. (2023). ^{236}U analyses with the ETH Zurich MILEA prototype system. *Nucl. Instruments Methods Phys. Res. Section B: Beam Interact. Materials Atoms* 534, 61–71. doi: 10.1016/j.nimb.2022.11.009

Christl, M., Vockenhuber, C., Kubik, P., Wacker, L., Lachner, J., Alfimov, V., et al. (2013). The ETH Zurich AMS facilities: Performance parameters and reference materials. *Nucl. Instruments Methods Phys. Res. Section B: Beam Interact. Materials Atoms* 294, 29–38. doi: 10.1016/j.nimb.2012.03.004

Clarke, R. A., and Gascard, J.-C. (1983). The formation of labrador sea water. part i: Large-scale processes. *J. Phys. Oceanography* 131764–1778. doi: 10.1175/1520-0485(1983)013⟨1764:TFOLSW⟩2.0.CO;2

Colombo, M., Rogalla, B., Myers, P. G., Allen, S. E., and Orians, K. J. (2019). Tracing dissolved lead sources in the canadian arctic: insights from the canadian GEOTRACES program. *ACS Earth Space Chem.* 3, 1302–1314. doi: 10.1021/acsearthspacechem.9b00083

Dahlgaard, H., Chen, Q., Herrmann, J., Nies, H., Ibbett, R., and Kershaw, P. (1995). On the background level of 99Tc, 90Sr and 137Cs in the North Atlantic. *J. Mar. Syst.* 6, 571–578. doi: 10.1016/0924-7963(95)00025-K

Dale, D., Christl, M., Vockenhuber, C., Macrander, A., Ólafsdóttir, S., Middag, R., et al. (2024). Tracing ocean circulation and mixing from the arctic to the subpolar north atlantic using the 129i–236u dual tracer. *J. Geophysical Research: Oceans* 129, e2024JC021211. doi: 10.1029/2024JC021211.E2024JC0212112024JC021211

Daniault, N., Mercier, H., Lherminier, P., Sarafanov, A., Falina, A., Zunino, P., et al. (2016). The northern North Atlantic Ocean mean circulation in the early 21st century. *Prog. Oceanography* 146, 142–158. doi: 10.1016/j.pocean.2016.06.007

De Steur, L., Hansen, E., Mauritzen, C., Beszczynska-Möller, A., and Fahrbach, E. (2014). Impact of recirculation on the east Greenland current in fram strait: Results from moored current meter measurements between 1997 and 2009. *Deep Sea Res. Part I: Oceanographic Res. Papers* 92, 26–40. doi: 10.1016/j.dsr.2014.05.018

Ditlevsen, P., and Ditlevsen, S. (2023). Warning of a forthcoming collapse of the Atlantic meridional overturning circulation. *Nat. Commun.* 14, 4254. doi: 10.1038/s41467-023-39810-w

Edmonds, H. N., Smith, J. N., Livingston, H. D., Kilius, L. R., and Edmond, J. M. (1998). 129I in archived seawater samples. *Deep Sea Res. Part I: Oceanographic Res. Papers* 45, 1111–1125. doi: 10.1016/S0967-0637(98)00007-7

Fogelqvist, E., Blindheim, J., Tanhua, T., Østerhus, S., Buch, E., and Rey, F. (2003). Greenland–scotland overflow studied by hydro-chemical multivariate analysis. *Deep Sea Res. Part I: Oceanographic Res. Papers* 50, 73–102. doi: 10.1016/S0967-0637(02)00131-0

Frajka-Williams, E., Ansorge, I. J., Baehr, J., Bryden, H. L., Chidichimo, M. P., Cunningham, S. A., et al. (2019). Atlantic meridional overturning circulation: observed transport and variability. *Front. Mar. Sci.* 6. doi: 10.3389/fmars.2019.00260

Furey, H., Bower, A., Ramsey, A., Houk, A., and Meunier, T. (2024). Variability of Iceland scotland overflow water across the reykjanes ridge: 2-years of moored

observations in the bight fracture zone. *JGR Oceans* 129, e2023JC020463. doi: 10.1029/2023JC020463

García-Ibáñez, M. I., Pardo, P. C., Carracedo, L. I., Mercier, H., Lherminier, P., Ríos, A. F., et al. (2015). Structure, transports and transformations of the water masses in the Atlantic Subpolar Gyre. *Prog. Oceanography* 135, 18–36. doi: 10.1016/j.pocean.2015.03.009

García-Ibáñez, M. I., Pérez, F. F., Lherminier, P., Zunino, P., Mercier, H., and Tréguer, P. (2018). Water mass distributions and transports for the 2014 GEOVIDE cruise in the North Atlantic. *Biogeosciences* 15, 2075–2090. doi: 10.5194/bg-15-2075-2018

Gou, R., Pennelly, C., and Myers, P. G. (2022). The changing behavior of the west Greenland current system in a very high-resolution model. *J. Geophysical Research: Oceans* 127. doi: 10.1029/2022JC018404

Håvik, L., Pickart, R. S., Våge, K., Torres, D., Thurnherr, A. M., Beszczynska-Möller, A., et al. (2017). Evolution of the east Greenland current from fram strait to Denmark strait: Synoptic measurements from summer 2012. *JGR Oceans* 122, 1974–1994. doi: 10.1002/2016JC012228

He, P., Hou, X., Aldahan, A., Possnert, G., and Yi, P. (2013). Iodine isotopes species fingerprinting environmental conditions in surface water along the northeastern atlantic ocean. *Sci. Rep.* 3, 2685. doi: 10.1038/srep02685

Holliday, N. P., Bacon, S., Allen, J., and McDonagh, E. L. (2009). Circulation and transport in the western boundary currents at cape farewell, Greenland. *J. Phys. Oceanogr.* 39, 1854–1870. doi: 10.1175/2009JPO4160.1

Holliday, N. P., Bersch, M., Berx, B., Chafik, L., Cunningham, S., Florindo-López, C., et al. (2020). Ocean circulation causes the largest freshening event for 120 years in eastern subpolar north atlantic. *Nat. Commun.* 11, 585. doi: 10.1038/s41467-020-14474-y

Holliday, N. P., Meyer, A., Bacon, S., Alderson, S., and de Cuevas, B. A. (2007a). The retroflection of part of the east Greenland current at cape farewell. *Geophys. Res. Lett.* 34, L07609. doi: 10.1029/2006GL029085

Holliday, N. P., Meyer, A., Bacon, S., Alderson, S. G., and de Cuevas, B. (2007b). Retroflection of part of the east Greenland current at Cape Farewell. *Geophysical Res. Lett.* 34, L07609. doi: 10.1029/2006GL029085

Johns, W. E., Devana, M., Houk, A., and Zou, S. (2021). Moored observations of the Iceland-scotland overflow plume along the eastern flank of the reykjanes ridge. *J. Geophysical Research: Oceans* 126. doi: 10.1029/2021JC017524

Kershaw, P., and Baxter, A. (1995). The transfer of reprocessing wastes from north-west Europe to the Arctic. *Deep Sea Res. Part II: Topical Stud. Oceanography* 42, 1413–1448. doi: 10.1016/0967-0645(95)00048-8

Lavender, K. L., Brechner Owens, W., and Davis, R. E. (2005). The mid-depth circulation of the subpolar North Atlantic Ocean as measured by subsurface floats. *Deep Sea Res. Part I: Oceanographic Res. Papers* 52, 767–785. doi: 10.1016/j.dsr.2004.12.007

Le Bihan, C., Lherminier, P., Le Bot, P., and Hamon, M. (2023). BOCATS 2021. Rapport de données CTD-O2. *ifremer*. doi: 10.13155/98984

Li, F., Lozier, M. S., Bacon, S., Bower, A. S., Cunningham, S. A., De Jong, M. F., et al. (20213002). Subpolar North Atlantic western boundary density anomalies and the Meridional Overturning Circulation. *Nat. Commun.* 12. doi: 10.1038/s41467-021-23350-2

Lilly, J. M., Rhines, P. B., Schott, F., Lavender, K., Lazier, J., Send, U., et al. (2003). Observations of the Labrador Sea eddy field. *Prog. Oceanography* 59, 75–176. doi: 10.1016/j.pocean.2003.08.013

Lin, P., Pickart, R. S., Jochumsen, K., Moore, G. W. K., Valdimarsson, H., Fristedt, T., et al. (2020). Kinematic structure and dynamics of the Denmark strait overflow from ship-based observations. *J. Phys. Oceanography* 503235–3251. doi: 10.1175/JPO-D-20-0095.1

Liu, M., and Tanhua, T. (2021). Water masses in the Atlantic Ocean: characteristics and distributions. *Ocean Sci.* 17, 463–486. doi: 10.5194/os-17-463-2021

Livingston, H. D., and Anderson, R. F. (1983). Large particle transport of plutonium and other fallout radionuclides to the deep ocean. *Nature* 303, 228–231. doi: 10.1038/303228a0

Lozier, M. S. (2023). Overturning in the subpolar north atlantic: a review. *Phil. Trans. R. Soc A.* 381, 20220191. doi: 10.1098/rsta.2022.0191

Lozier, M. S., Gary, S. F., and Bower, A. S. (2013). Simulated pathways of the overflow waters in the North Atlantic: Subpolar to subtropical export. *Deep Sea Res. Part II: Topical Stud. Oceanography* 85, 147–153. doi: 10.1016/j.dsr2.2012.07.037

Lozier, M. S., Li, F., Bacon, S., Bahr, F., Bower, A. S., Cunningham, S. A., et al. (2019). A sea change in our view of overturning in the subpolar North Atlantic. *Science* 363, 516–521. doi: 10.1126/science.aau6592

Michel, R., Daraoui, A., Gorny, M., Jakob, D., Sachse, R., Tosch, L., et al. (2012). Iodine-129 and iodine-127 in European seawaters and in precipitation from Northern Germany. *Sci. Total Environ.* 419, 151–169. doi: 10.1016/j.scitotenv.2012.01.009

Olsson, K. A., Jeansson, E., Tanhua, T., and Gascard, J.-C. (2005). The East Greenland Current studied with CFCs and released sulphur hexafluoride. *J. Mar. Syst.* 55, 77–95. doi: 10.1016/j.jmarsys.2004.07.019

Pacini, A., and Pickart, R. S. (2022). Meanders of the west Greenland current near cape farewell. *Deep Sea Res. Part I: Oceanographic Res. Papers* 179, 103664. doi: 10.1016/j.dsr.2021.103664

Payne, A., Wefing, A., Christl, M., Vockenhuber, C., Williams, W., Smith, J. N., et al. (2024). Circulation timescales and pathways of atlantic water in the Canada basin: Insights from transient tracers [129]i and [236]u. *JGR Oceans* 129, e2023JC020813. doi: 10.1029/2023JC020813

Pickart, R. S. (1992). Water mass components of the north atlantic deep western boundary current. *Deep Sea Res. Part A. Oceanographic Res. Papers* 39, 1553–1572. doi: 10.1016/0198-0149(92)90047-W

Poole, R., and Tomczak, M. (1999). Optimum multiparameter analysis of the water mass structure in the atlantic ocean thermocline. *Deep Sea Res. Part I: Oceanographic Res. Papers* 46, 1895–1921. doi: 10.1016/S0967-0637(99)00025-4

Raisbeck, G., and Yiou, F. (1999). 129I in the oceans: origins and applications. *Sci. Total Environ.*, 237–238. doi: 10.1016/S0048-9697(99)00122-9

Rhein, M., Kieke, D., Hüttl-Kabus, S., Roessler, A., Mertens, C., Meissner, R., et al. (2011). Deep water formation, the subpolar gyre, and the meridional overturning circulation in the subpolar North Atlantic. *Deep Sea Res. Part II: Topical Stud. Oceanography* 58, 1819–1832. doi: 10.1016/j.dsr2.2010.10.061

Rousi, E., Selten, F., Rahmstorf, S., and Coumou, D. (2021). Changes in north atlantic atmospheric circulation in a warmer climate favor winter flooding and summer drought over europe. *J. Climate* 34, 2277–2295. doi: 10.1175/JCLI-D-20-0311.1

Rudels, B. (2002). The east Greenland current and its contribution to the Denmark strait overflow. *ICES J. Mar. Sci.* 59, 1133–1154. doi: 10.1006/jmsc.2002.1284

Rudels, B., Eriksson, P., Grönvall, H., Hietala, R., and Launiainen, J. (1999). Hydrographic observations in Denmark strait in fall 1997, and their implications for the entrainment into the overflow plume. *Geophysical Res. Lett.* 26, 1325–1328. doi: 10.1029/1999GL900212

Sakaguchi, A., Kadokura, A., Steier, P., Takahashi, Y., Shizuma, K., Hoshi, M., et al. (2012). Uranium-236 as a new oceanic tracer: A first depth profile in the Japan Sea and comparison with caesium-137. *Earth Planetary Sci. Lett.* 333 (334), 165–170. doi: 10.1016/j.epsl.2012.04.004

Smethie, W. M., Fine, R. A., Putzka, A., and Jones, E. P. (2000). Tracing the flow of North Atlantic Deep Water using chlorofluorocarbons. *J. Geophys. Res.* 105, 14297–14323. doi: 10.1029/1999JC900274

Smith, J. N. (2005). Iodine 129/CFC 11 transit times for Denmark Strait Overflow Water in the Labrador and Irminger Seas. *J. Geophysical Res.* 110, C05006. doi: 10.1029/2004JC002516

Smith, J. N., Ellis, K. M., and Kilius, L. R. (1998). 129I and 137Cs tracer measurements in the Arctic Ocean. *Deep Sea Res. Part I: Oceanographic Res. Papers* 45, 959–984. doi: 10.1016/S0967-0637(97)00107-6

Smith, J. N., McLaughlin, F. A., Smethie, W. M., Moran, S. B., and Lepore, K. (2011). Iodine-129, ^{137}Cs, and CFC-11 tracer transit time distributions in the Arctic Ocean. *J. Geophysical Res.* 116, C04024. doi: 10.1029/2010JC006471

Stramma, L., Kieke, D., Rhein, M., Schott, F., Yashayaev, I., and Koltermann, K. P. (2004). Deep water changes at the western boundary of the subpolar north atlantic during 1996 to 2001. *Deep Sea Res. Part I: Oceanographic Res. Papers* 51, 1033–1056. doi: 10.1016/j.dsr.2004.04.001

Susan Lozier, M., Bacon, S., Bower, A. S., Cunningham, S. A., Femke De Jong, M., De Steur, L., et al. (2017). Overturning in the subpolar north atlantic program: A new international ocean observing system. *Bull. Am. Meteorological Soc.* 98, 737–752. doi: 10.1175/BAMS-D-16-0057.1

Susan Lozier, M., Bower, A. S., Furey, H. H., Drouin, K. L., Xu, X., and Zou, S. (2022). Overflow water pathways in the North Atlantic. *Prog. Oceanography* 208, 102874. doi: 10.1016/j.pocean.2022.102874

Sutherland, D. A., Pickart, R. S., Peter Jones, E., Azetsu-Scott, K., Jane Eert, A., and d Olafsson, J. (2009). Freshwater composition of the waters off southeast Greenland and

their link to the Arctic Ocean. *J. Geophysical Res.* 114, C05020. doi: 10.1029/2008JC004808

Tanhua, T. (2005). Spreading of overflow water from the Greenland to the Labrador Sea. *Geophys. Res. Lett.* 32, L10605. doi: 10.1029/2005GL022700

Tanhua, T., Olsson, K. A., and Jeansson, E. (2005). Formation of Denmark Strait overflow water and its hydro-chemical composition. *J. Mar. Syst.* 57, 264–288. doi: 10.1016/j.jmarsys.2005.05

Våge, K., Pickart, R. S., Spall, M. A., Moore, G., Valdimarsson, H., Torres, D. J., et al. (2013). Revised circulation scheme north of the Denmark strait. *Deep Sea Res. Part I: Oceanographic Res. Papers* 79, 20–39. doi: 10.1016/j.dsr.2013.05.007

Vockenhuber, C., Casacuberta, N., Christl, M., and Synal, H.-A. (2015). Accelerator Mass Spectrometry of [129]I towards its lower limits. *Nucl. Instruments Methods Phys. Res. Section B: Beam Interact. Materials Atoms* 361, 445–449. doi: 10.1016/j.nimb.2015.01.061

Wefing, A.-M., Casacuberta, N., Christl, M., and Dodd, P. A. (2022). Water mass composition in Fram Strait determined from the combination of [129]I and [236]U: Changes between 2016, 2018, and 2019. *Front. Mar. Sci.* 9. doi: 10.3389/fmars.2022.973507

Wefing, A.-M., Casacuberta, N., Christl, M., Gruber, N., and Smith, J. N. (2021). Circulation timescales of Atlantic Water in the Arctic Ocean determined from anthropogenic radionuclides. *Ocean Sci.* 17, 111–129. doi: 10.5194/os-17-111-2021

Wefing, A., Christl, M., Vockenhuber, C., Rutgers van der Loeff, M., and Casacuberta, N. (2019). Tracing atlantic waters using [129]I and [236]U in the fram strait in 2016. *J. Geophysical Research: Oceans* 124, 882–896. doi: 10.1029/2018JC014399

Weijer, W., Haine, T., Siddiqui, A., Cheng, W., Veneziani, M., and Kurtakoti, P. (2022). Interactions between the arctic mediterranean and the atlantic meridional overturning circulation: A review. *Oceanog.* 35 (3–4), 118–127. doi: 10.5670/oceanog.2022.130

Xu, X., Rhines, P. B., Chassignet, E. P., and Schmitz, W. J. (2015). Spreading of Denmark strait overflow water in the western subpolar north atlantic: insights from eddy-resolving simulations with a passive tracer. *J. Phys. Oceanography* 45, 2913–2932. doi: 10.1175/JPO-D-14-0179.1

Yashayaev, I. (2007). Changing freshwater content: Insights from the subpolar North Atlantic and new oceanographic challenges. *Prog. Oceanography* 73, 203–209. doi: 10.1016/j.pocean.2007.04.014

Yashayaev, I. (2024). Intensification and shutdown of deep convection in the labrador sea were caused by changes in atmospheric and freshwater dynamics. *Commun. Earth Environ.* 5, 156. doi: 10.1038/s43247-024-01296-9

Zhang, Y., Chen, C.-S., Shen, X.-Y., Xu, D.-Y., Shao, W.-Z., Beardsley, R. C., et al. (2021b). Role of sea level pressure in variations of the canadian arctic archipelago throughflow. *Adv. Climate Change Res.* 12, 539–552. doi: 10.1016/j.accre.2021.07.009

Zhang, J., Weijer, W., Steele, M., Cheng, W., Verma, T., and Veneziani, M. (2021a). Labrador Sea freshening linked to Beaufort Gyre freshwater release. *Nat. Commun.* 12, 1229. doi: 10.1038/s41467-021-21470-3

Zou, S., Bower, A. S., Lozier, M. S., and Furey, H. H. (2023). Deep ocean circulation in the subpolar north atlantic observed by acoustically-tracked floats. *Prog. Oceanography* 211, 102975. doi: 10.1016/j.pocean.2023.102975

Zou, S., Petit, T., Li, F., and Lozier, M. S. (2024). Observation-based estimates of water mass transformation and formation in the labrador sea. *J. Phys. Oceanography*. 54, 1411–1429. doi: 10.1175/JPO-D-23-0235.1

Zunino, P., Lherminier, P., Mercier, H., Daniault, N., García-Ibáñez, M. I., and Pérez, F. F. (2017). The GEOVIDE cruise in May–June 2014 reveals an intense Meridional Overturning Circulation over a cold and fresh subpolar North Atlantic. *Biogeosciences* 14, 5323–5342. doi: 10.5194/bg-14-5323-2017

Appendix A: Acronyms

Acronyms of water masses, geographic locations, and
radionuclide sources.

AABW	Antarctic Bottom Water
AAW	Arctic Atlantic Water
AMOC	Atlantic Meridional Overturning Circulation
AMS	Accelerator Mass Spectrometry
BIC	Baffin Island Current
DSOW	Denmark Strait Overflow Water
EGC	East Greenland Current
ENACW	Eastern North Atlantic Central Water
IcB	Icelandic Basin
IrS	Irminger Sea
ISOW	Iceland–Scotland Overflow Water
LC	Labrador Current
LS	Labrador Sea
LSW	Labrador Sea Water
MW	Mediterranean Water
NAC	North Atlantic Current
NEADW	North East Atlantic Deep Water
NEABW	North East Atlantic Bottom Water
PSW	Polar Surface Water
RAW	Recirculating Atlantic Water
RetAW	Return Atlantic Water
SPMW	Subpolar Mode Water
SPNA	Subpolar North Atlantic
WEB	West European Basin
WGC	West Greenland Current